How to cite: *Angew. Chem. Int. Ed.* **2022,** *61,* e202208016
International Edition: doi.org/10.1002/anie.202208016
German Edition: doi.org/10.1002/ange.202208016

Nanoparticles

Direct Dry Synthesis of Supported Bimetallic Catalysts: A Study on Comminution and Alloying of Metal Nanoparticles

*Jacopo De Bellis, Hilke Petersen, Jan Ternieden, Norbert Pfänder, Claudia Weidenthaler, and Ferdi Schüth**

Abstract: Ball milling is growing increasingly important as an alternative synthetic tool to prepare catalytic materials. It was recently observed that supported metal catalysts could be directly obtained upon ball milling from the coarse powders of metal and oxide support. Moreover, when two compatible metal sources are simultaneously subjected to the mechanochemical treatment, bimetallic nanoparticles are obtained. A systematic investigation was extended to different metals and supports to understand better the mechanisms involved in the comminution and alloying of metal nanoparticles. Based on this, a model describing the role of metal-support interactions in the synthesis was developed. The findings will be helpful for the future rational design of supported metal catalysts via dry ball milling.

Introduction

Supported metal catalysts represent the most important class of materials for industrial catalysis applications.[1] Among others, supported catalysts based on alloys, i.e., where the active phase comprises two or more intimately mixed metallic components, are becoming increasingly relevant due to the possible occurrence of synergistic effects.[2] Notably, it has already been observed that the activity, selectivity, or stability of alloys often exceeds the sum of activities, selectivities, or stabilities of the metallic constituents, which is highly appealing.[3] A striking example comes from a recent study by the groups of Hutchings and Kiely, where enhanced rates were noted in the oxidative dehydrogenation of hydroxymethylfurfural depending on the composition and mixing pattern of Au and Pd in the catalyst material.[4] However, several other examples can be found in the literature.[5]

Many different methods are available to synthesize supported metal catalysts, including bimetallic formulations. Most methods are solution-based, such as wet impregnation, coprecipitation, deposition-precipitation, and colloidal synthesis.[6] In general, the chemical reduction or thermal decomposition of suitable metal precursors (e.g., water-soluble inorganic salts and organic metal complexes) is the target of the synthesis. This is carried out in the presence of the chosen support or in conjunction with its formation. Thus, the manufacture of supported metal catalysts involves the use of a large amount of solvents and several process control agents, including buffers, capping agents (surfactants), reducing agents, and many others.[7] Furthermore, after filtration and drying, post-synthesis thermal treatments (e.g., calcination, reduction, and annealing) are usually required to remove possible residues of the additives used during the synthesis or as the last step to attain the final most performant form of the material. While high-performance catalysts are customarily obtained via such wet chemistry processes, this often comes at the expense of complex processing and associated high costs. To circumvent these sophisticated synthetic methods, alternative methodologies are required to simplify procedures in catalyst synthesis.

Mechanochemical methods, primarily dominated by the practice of ball milling, are therefore becoming increasingly popular, as they provide easy access to a wide range of relevant catalytic materials at a lower cost and minor environmental impact.[8] For instance, in our group, a mechanochemical method was recently developed to synthesize supported metal catalysts simply from the coarse powders of the metal and oxide support.[9] Briefly, when Au was ball milled in the presence of the oxide support in a high-energy regime, the formation of supported Au nanoparticles was observed. Interestingly, the method proved to have general applicability, as it was extended to several other metals and oxide supports. Moreover, the approach was also successfully applied to the preparation of supported bimetallic nanoparticles, with the examples of PdAu and CuAu alloy nanoparticles on MgO and yttria-stabilized zirconia as representative oxide supports.[10] Supported alloy nanoparticles are formed by simply combining two compatible metal sources at the same time. As a side remark, all

[*] Dr. J. De Bellis, Dr. H. Petersen, J. Ternieden, Dr. C. Weidenthaler, Prof. Dr. F. Schüth
Department of Heterogeneous Catalysis, Max-Planck-Institut für Kohlenforschung
Kaiser-Wilhelm-Platz 1, 45470 Mülheim an der Ruhr (Germany)
E-mail: schueth@kofo.mpg.de
N. Pfänder
Department of Heterogeneous Reactions, Max-Planck-Institut für Chemische Energiekonversion
Stiftstraße 34–36, 45470 Mülheim an der Ruhr (Germany)

the materials were investigated as catalysts in CO oxidation, a simple model reaction, and they show similar behavior to their conventionally synthesized counterparts. This demonstrates the value of the methodology as a means to catalyst synthesis. This notion was further corroborated by other similar case studies that have recently appeared in the literature.[11]

However, in contrast to solution-based techniques, where the effect of different parameters on the properties of final materials has been investigated in some detail, it is yet not clear how solid-state transformations are induced upon ball milling. Particularly, there are several open questions: first, on the most basic level, it is unclear how comminution of different metals proceeds on oxide supports upon ball milling to such an extent that eventually the formation of metal nanoparticles is observed even under relatively mild milling conditions.[9–11,12] It is also rather intriguing to observe that metal comminution is strongly affected by the nature of the oxide support so that different metal dispersions are obtained depending on the specific system.[9] Similarly, different metals and their combinations (as alloys) would spread differently on given oxide support when subjected to the same treatment.[9,10] Finally, alloying of metal nanoparticles upon ball milling represents a somewhat puzzling phenomenon per se, which requires further investigation.

In the present work, a model for the mechanochemical synthesis of supported metal nanoparticles, including mono- and bimetallic formulations, is described, considering the results of a systematic investigation extended to many different metals (alone and in combination) and metal oxide supports. In brief, the overall process, including comminution-deposition of metal nanoparticles and alloying (on occasion), can be described in terms of recently updated theories of mechanochemical mixing of solid particles.[13] Furthermore, some important trends in the comminution and alloying of different metal nanoparticles were systematically studied, which could help in the rational design of mono- and bimetallic supported catalysts via mechanochemical methods.

Results and Discussion

In order to develop a better understanding of the ball milling synthesis of supported metal catalysts, Pd, Ag, Pt, and Au were ball milled alone or in combination in the presence of MgO as support. While the choice of metals was mainly motivated by their relevance as catalytic metals, MgO was preferred as the support for the ease of analysis of the resulting materials, i.e., for the little overlap of the reflections in the X-ray diffraction (XRD) patterns and reasonably different electron densities of the components to allow good discrimination of separate phases under the electron microscope. However, the synthesis of PdAu nanoparticles was also reproduced with $MgAl_2O_4$, α-Al_2O_3, and α-Fe_2O_3 as supports to study the support influence. Unless otherwise specified, all syntheses were carried out under the same milling conditions to set reasonable grounds for comparison. Particularly, the coarse powders of the metal(s) and oxide support were ball-milled in a 15 mL stainless steel milling jar (shaker mill fit) at 25 Hz using two big grinding balls (15 mm Ø) for different milling times. The same concentration of metal(s) was used for all the syntheses (1 g scale). Finally, all the preparations were carried out in air under normal pressure. In the following sections, PdAu and PdAg nanoparticles on MgO as support and their monometallic counterparts will be studied first as benchmark systems.

As seen from the broadening of the reflections typical for Pd and Au (Figure 1a) and Pd and Ag (Figure 1b), the process first proceeds through the seemingly independent comminution of the metal components. Indeed, no meaningful difference was noted in the line profiles for the case where Pd, Ag, and Au were milled with MgO and no other metal present at the same time (superimposed dashed lines). Thus, smaller metal particles are separated from the bulk metal and mixed with the MgO particles or supported on this latter, resulting in a homogeneous powder mixture. It has already been demonstrated that when hard and soft, brittle and plastic samples are processed together, such as metal(s) and metal oxide powders, the harder component (the oxide support) can act as the grinding body towards the soft and plastic one (the metal). The metal is thus subjected to activation by deformation, which will lead to the latter being smeared over the former.[13] In our case, this notion was corroborated by the step-wise increase of the Pd, Ag, and Au content in the samples up to 60 min of ball milling, as seen from the intensification of the diffraction lines and determined via SEM-EDX bulk elemental analysis of the samples (Figure 1c,d). The fraction not detected remains likely segregated from the bulk powder and adheres to the walls of the milling jar and the balls, as also detected by visual inspection after short milling times. No significant difference was observed in the metal uptake of the support vs. milling time for the different metals or mixtures of metals.

On the other hand, comminution rates slightly differ, as noted from the relative variation of average crystallite sizes determined by applying the whole powder pattern modeling (WPPM) approach to the powder XRD patterns of the samples,[14] especially within the first 90 min of milling (Figure 2a). Accordingly, the noble metals showed an increasing tendency towards comminution following the order Pd < Au < Ag, seemingly in agreement with the stress required to induce twinning (a common deformation mechanism) across the series of *fcc*-metals.[15] Notwithstanding, comminution rates slightly differ, as noted from the relative variation of average crystallite sizes determined by applying the WPPM approach. However, a note of caution is due here since metal powders with slightly different coarseness were used for the study. For instance, Pt appears to comminute more quickly than Pd (Figure S8), compatible with the smallest initial particle size for Pt (more information under Experimental Methods in Supporting Information), but in contrast to expectations. Independent corroboration of these trends by electron microscopy was not possible, unfortunately, because the formation of supported

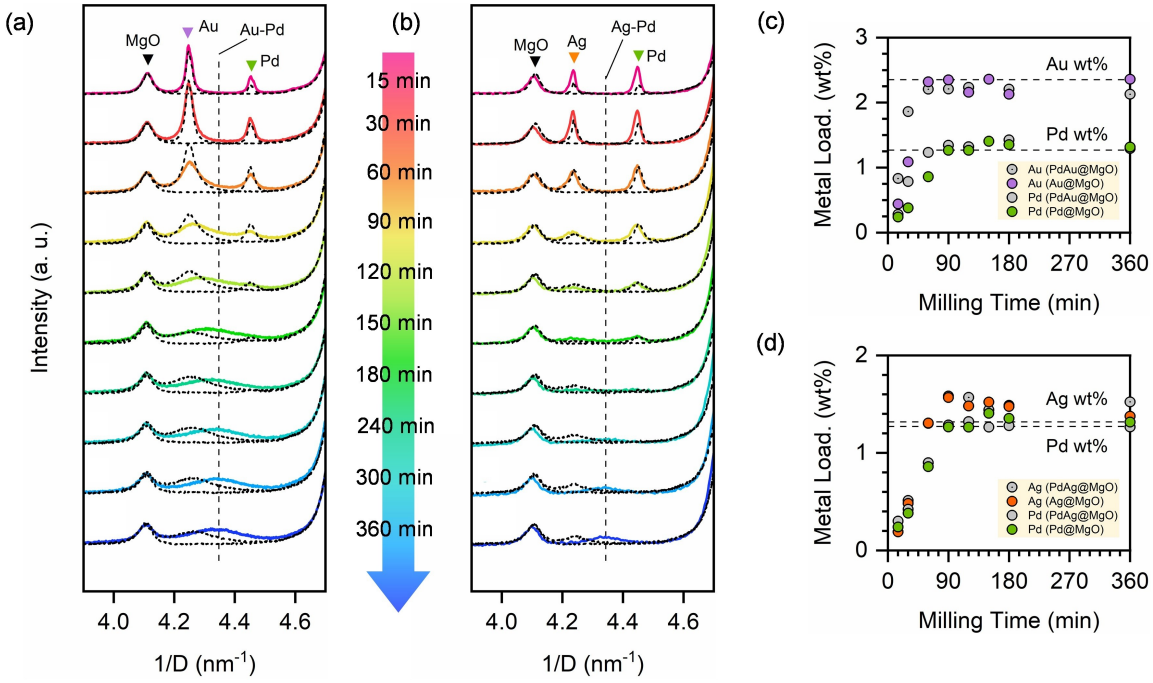

Figure 1. a,b) As colored solid lines, the powder XRD patterns of 1.0 mol% PdAu@MgO (a) and PdAg@MgO (b) measured after increasing milling times (as specified). Superimposed dashed black lines correspond to the powder XRD patterns of 0.5 mol% Au@MgO and Pd@MgO (a) or Ag@MgO and Pd@MgO (b), similarly measured after longer milling times. All the XRD patterns are plotted in relative intensity, i.e., to the intensity of the most prominent reflection for the support, and then stacked given a fixed y-shift. The most prominent reflections for the crystalline phases detected in the samples are marked. Dashed vertical lines indicate the position of the reflections expected for an AuPd (1 : 1) or AgPd (1 : 1) alloy, accordingly.[17] Full range XRD patterns for PdAu@MgO and PdAg@MgO are reported in *Supporting Information* as Figure S2 and Figure S4. Uptake of Au and Pd on MgO (also referred to as metal loading) for Au@MgO, PdAu@MgO, and Pd@MgO (c) and Ag and Pd on MgO for Pd@MgO, AgPd@MgO, and Au@MgO (d) after increasing milling times as determined via SEM-EDX bulk elemental analysis of milled powders (Table S3). The plotted values are corrected for the amount of Fe present in the sample due to abrasion of the milling jar and balls (Table S4). Dashed horizontal lines indicate the target metal loading.

nanoparticles was only observed after about 60 min of ball milling when the maximum metal uptake was also measured (Figure 2b). Therefore, for short milling times, the analysis of the samples via electron microscopy was highly unreliable.

As a side remark, average crystallite sizes determined by applying the WPPM approach to the XRD patterns do not match particle sizes found during the investigation of the samples under the electron microscope but are systematically smaller. This is not surprising because the WPPM approach considers the size distribution of columns of undistorted unit cells, thus defining the coherently scattering domains present within metal particles across the sample. Indeed, particles often consist of multiple such coherently scattering domains (polycrystallinity).[16] Independently, it is also important to note that the approach has intrinsic limitations connected with the quality of the data, i.e., the possible lack of contrast between the intensity of target reflections and the overall scattering. The results, therefore, need to be interpreted with caution; while trends are most probably correct, absolute values may carry a substantial error. More information on the method is provided in Supporting Information under Experimental Methods.

The first indications of alloying were observed after about 90 min. Tailing of the XRD reflections, most evident when compared with the case where only one metal was processed at a time, points to the gradual dissolution of one metal component into the other and vice versa (Figure 1a,b). Interestingly, except for a slightly narrower particle size distribution, no significant difference was observed in the dispersion of Pd, Ag, and Au nanoparticles on MgO after 60 and 90 min of ball milling (Figure S13–14). Under the assumption that metal comminution proceeds independently before alloying is observed, the previous evidence suggests that no critical particle size is required to initiate alloying. Thus, alloying might occur even during the earlier stages of the process (within the first 60 min); however, it would become statistically more relevant—and thus detectable by XRD—only when a high level of metal dispersion is attained across the system ($d_{TEM} < 10$ nm, Figure 2b). From the first indication of alloying onwards, alloying proceeds further so that metal species with increasing content of the second metal are formed (as solid solutions).[17] Interestingly, no clear indication of preferential mixing was noted from the XRD patterns, although dissolution of Pd into Au and Ag is supposed to be more favorable than vice versa.[18] The same conclusions were reached even when a higher total metal loading (2-fold) was used to facilitate monitoring of possible underlying processes (Figure S1). Still, it is important to note that the contribution from unreacted Pd to the XRD

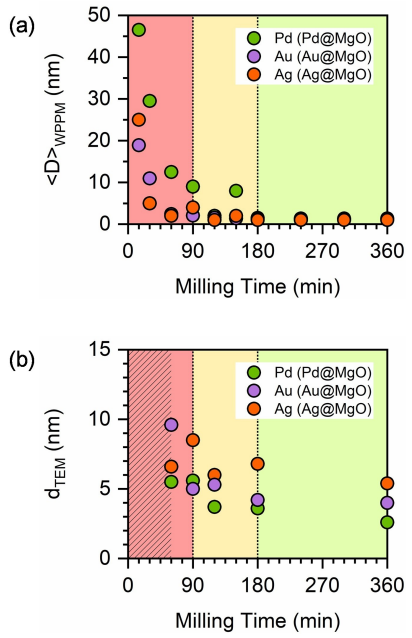

Figure 2. a) Average size (diameter, D) of Ag, Au, and Pd coherently scattering domains (crystallites) on MgO support for increasing milling times (from t_0 to 360 min) as determined by applying the WPPM approach (Figure S8 includes Pt on MgO). b) Average size (diameter, d) of Ag, Au, and Pd nanoparticles on MgO for increasing milling times (from 60 to 360 min) as established from corresponding micrographs (TEM). The complete particle size distributions (histograms) are reported in *Supporting Information* in Figure S13 and Figure S14. From left to right in (a) and (b), the colored ranges define approximate limits of the comminution stage (red), alloying phase (yellow), and steady-state regime (green) possibly occurring during the mechanochemical synthesis of supported bimetallic nanoparticles (on MgO).

patterns was always more easily detected than the one from Au and Ag during alloying (Figure 1a,b).

For the PdAu system, the steady-state, meaning the formation of alloy species with target composition, was achieved after about 180 min of milling. For the PdAg system, the steady-state was achieved slightly later, possibly due to the lower enthalpy of mixing for Pd and Ag compared to Pd and Au.[17] Small deviations from nominal compositions were always observed, as seen from the position of the XRD reflections. Also, the wide broadening of the diffraction lines suggested compositional inhomogeneities. Nevertheless, the EDX line scans recorded on alloy nanoparticles only indicated minor deviations from the target composition in all cases (vide infra). Therefore, size effects possibly play a major role in determining the breadth of the diffraction line profile. After reaching the steady-state, further milling did not produce any significant changes in the system up to 360 min, when milling was stopped—at least according to the characterization of the samples via XRD—in agreement with previous findings.[10]

To summarize the main findings up to this point: when Pd and Au or Pd and Ag are ball-milled in the presence of MgO, first, monometallic metal nanoparticles are formed via comminution, possibly under the action of MgO itself as the grinding body. By these means, a homogeneous solid mixture is slowly attained. The deposition of metal nanoparticles onto the MgO support can be observed only when a sufficiently high dispersion has been attained for the metal components. Shortly after this point, alloying is also noted for the first time. Alloying seems to proceed by the gradual dissolution of one component into the other until an equilibrium is reached and the average composition is obtained (steady-state).

Similar considerations also apply to the case of PtAu, AgAu, and PdPt nanoparticles supported on MgO, including the induction period before alloying and waiting time until a steady-state is finally attained, provided that similar experimental conditions are applied. All the results from the characterization of the samples via XRD (time profiles) and electron microscopy are available as Supporting Information (Table S5, Figure S5–S7, Figure S16). In all cases, including PdAu and PdAg-based systems, the formation of nanosized (supported) alloy species—already pointed out by the position and shape of the diffraction lines—was confirmed by direct observation of the nanoparticles by electron microscopy, and alloying was further corroborated by a series of EDX line scans (Figure S15–16). No sign of surface segregation was noted for the alloy nanoparticles by these means.

We speculate for alloying to occur via the occasional coalescence of immobilized metal nanoparticles supported on the MgO particles upon collision (Scheme 1). If the energy by which the nanoparticles are brought into contact is sufficiently high, such nanoparticles could fuse and intermix upon impact (Scheme 1a), as has already been predicted for isolated metal nanoclusters.[19] However, by similar means, the nanoparticles might be pulled apart (Scheme 1b) and divided once more (Scheme 1c), but atoms could interdiffuse in the merged state. The repetition of such a mechanism would eventually lead to the formation of alloy species with a composition compatible with the available amount of each monometallic precursor. This model would only work if metal-support interactions are strong enough to outweigh metal-metal interactions in determining the kinetically-limited structures that are possibly achieved here (vide infra), as seems to be the case. Otherwise, metal comminution and subsequent deposition on the support could not occur to the extent observed. Without such an influence, steady-state particle sizes upon ball milling are more in the range of several hundred nanometers to micrometers.[20] Finally, it is also conceivable that individual metal nanoparticles could be transferred from one support particle to the other upon impact when trapped between two of them, according to their relative "sticking" probability. Such a mechanism would likely contribute to the homogeneous distribution of supported metal nanoparticles.

In this picture, the rate of alloying would significantly depend upon mixing conditions, i.e., milling frequency. Indeed, the steady-state was consistently delayed when the milling frequency was lowered from 25 to 15 Hz (Figure S3). However, since alloying of Au and Pd was observed even at frequencies as low as 15 Hz, no energetic threshold requirements could be determined.

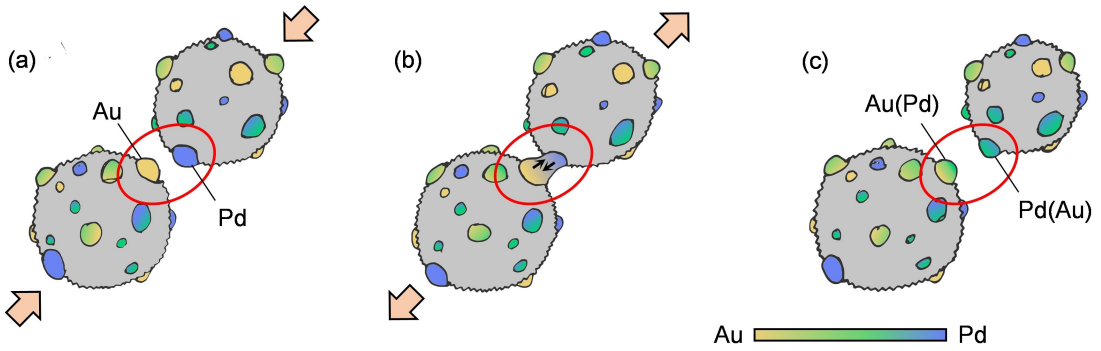

Scheme 1. Proposed mechanism for the coalescence of supported metal nanoparticles upon ball milling exemplified by Au and Pd on MgO support. During one collision event: a) Au and Pd metal nanoparticles supported on separated MgO particles (in grey) are brought into contact; b) Au and Pd atoms interdiffuse in the merged state before the parts are divided again by the field of forces in action; c) Au(Pd) and Pd(Au) species are formed. The color gradient represents the degree of mixing, with Au on the yellow side and Pd on the blue side of the scale.

It is unclear what conditions are generated between colliding balls, particularly for closely interacting solid particles. Several theories and models have already been outlined to explain how solid-state reactions can occur upon mechanochemical activation.[21] Still, a comprehensive understanding of the phenomenon has not yet been achieved. The newly developed methods for monitoring mechanochemical reactions, e.g., via synchrotron X-ray powder diffraction, Raman spectroscopy, X-ray absorption spectroscopy, and solid-state NMR, will possibly help gather more evidence of underlying mechanisms and cast new light on the problem.[22]

It is important to note that Fe was found in all the samples due to the abrasion of the milling jar and balls (Table S4 and Table S6). In general, the amount of Fe in the samples increased linearly with the milling time up to about 10 wt% after 360 min of ball milling. The longer the vessels had been in use, the more severe this phenomenon was, as seen for data after 360 min of milling sorted by date of the experiment (Figure S12). Since no correlation with the nature of the noble metal(s) used, either alone or in combination, was observed, selective abrasion of iron from the equipment was excluded. Moreover, in all cases, the position of the XRD reflections was consistent with the formation of the target alloy species, so no indication was found that Fe alloyed with the noble metals. This applies especially to the case of Pd and Pt, where a favorable enthalpy of mixing could lead to the formation of Pd(Fe) and Pt(Fe) alloy species, respectively.[23] The EDX line scans further corroborated this notion as constant levels of Fe were detected across the samples, thus excluding its selective incorporation in the alloys (Figure S15–16).

Contamination of catalyst materials by iron would certainly be a disadvantage. Thus, the use of ceramic-based milling tools and alternative milling devices (e.g., planetary ball mills) is currently under investigation. Preliminary results suggest that materials with similar features can be produced as with the steel equipment after appropriate adaptation of the parameters.

The ball milling synthesis method proved to be suitable for very diverse combinations of metals, leading to the formation of alloy nanoparticles in all cases. Particularly, the formation of hard-to-synthesize PdPt and PtAu disordered alloys upon ball milling was somewhat unexpected because PdPt and PtAu solid solutions are known to form only at very high temperatures, i.e., above 800 °C for PdPt and above 1200 °C for PtAu bulk alloys.[24] Furthermore, previous attempts to synthesize PdPt and PtAu nanoalloys have primarily resulted in the formation of core–shell structures with the metal with the lowest surface energy typically segregating to the surface.[25] Our observations thus suggest that hard-to-synthesize nanoalloys are accessible via ball milling. This may even include combinations for which a miscibility gap exists, provided suitable milling conditions are applied. This has already been extensively demonstrated in the case of bulk alloys.[26] Thus, ball milling offers the means to expand the scope of materials that can potentially be investigated for catalysis applications. Finally, easy access to a wide variety of materials could also be exploited to understand better the phenomena involved in the preparation of supported metal catalysts.

Systematic trends were observed when the size distribution of monometallic and bimetallic nanoparticles on MgO was studied (Figure 3). Increasing average particle sizes were determined for supported Pt, Pd, Au, and Ag nanoparticles after 360 min of ball milling with MgO as the support. In the same order, the standard deviation also increases so that a broader size distribution is observed when moving from Pt to Ag along the series. Thus, while an average particle size of about 2 nm and standard deviation of around 1 nm was determined for Pt, an average particle size of 5 nm and standard deviation of around 2 nm was estimated for Ag on MgO at the opposite side of the series (precise values are reported in Table S7). With a high level of statistical significance, the following order for the average sizes of noble metal nanoparticles on MgO can be given: $Pt < Pd < Au \approx Ag$.

These findings would support the notion that different sizes are expected for supported metal nanoparticles accord-

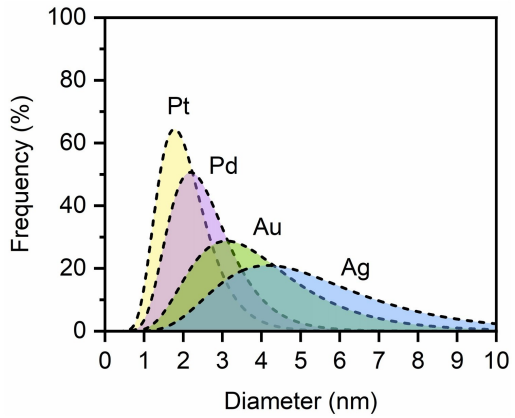

Figure 3. Comparison of the size distribution curves for monometallic Pt, Pd, Au, and Ag nanoparticles on MgO support after 360 min of ball milling. The best-fitting lognormal distribution curves around related histograms in Figure S17 are plotted in all cases.

ing to the relative affinity of the metals for the support (oxophilicity, defined as heat of formation of the most stable oxide of metal element M from one gaseous M atom plus O_2), which would roughly correlate with interfacial energies.[27] It has already been demonstrated that the adhesion energies of noble metals on a flat MgO surface scale linearly with the metal oxophilicity.[28] Since metal oxophilicity increases in the order $Ag < Au < Pd < Pt$, it similarly applies to the adhesion energies of such metals on the MgO support and, along with it, the relative stability of small (supported) metal particles.

A systematic behavior was also observed in the case of alloy nanoparticles. Particularly, for all the bimetallic formulations, the mean and standard deviation of the particle size distribution would reproducibly assume values between those determined for the size distribution of the monometallic counterparts (Table S7). This can be better visualized by directly comparing the particle size distributions, case by case. For instance, as shown in Figure 4a, the size distribution of PtAu nanoparticles appears as a combination of the size distribution of Pt and Au nanoparticles. The same holds for PdAg and PdAu (Figure 4b,c). For PdPt (Figure 4d) and AgAu (Figure 4e) nanoparticles, the differences to the monometallic counterparts are less pronounced since the distributions for the monometallic samples are quite similar, but the correlation is still rather obvious. Possibly, the considerations previously applied to the supported noble metal nanoparticles might also be valid when corresponding combinations are taken into account. This is most evident when the particle size distributions of Pd, PdPt, PdAu, and PdAg are compared (Figure 4f). The mean values appear to increase with the oxophilicity of the second metal (Pt, Au, and Ag) decreasing, as in the case of the monometallic particles. However, this situation had not been considered in the study mentioned above.[28]

This hypothesis is further corroborated by the lower average particle size determined for AuPd nanoparticles on α-Fe_2O_3 (Table S8 and Figure S18), compatible with the

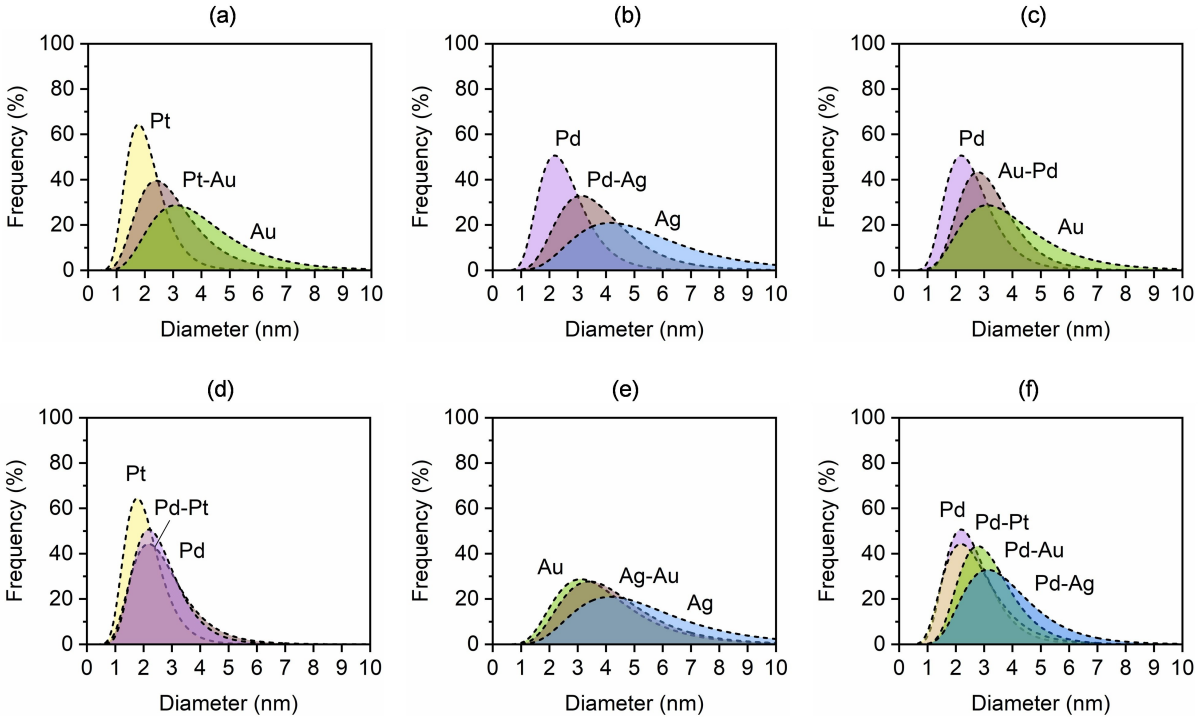

Figure 4. The size distribution curves for bimetallic PtAu (a), PdAg (b), PdAu (c), PdPt (d), and AgAu (e) nanoparticles on MgO support are compared to the size distribution curves obtained for the corresponding monometallic counterparts. Comparison of the size distribution curves of PdPt, Pd, PdAu, and PdAg nanoparticles on MgO support (f). The best-fitting lognormal distribution curves around related histograms from Figure S17 are plotted in all cases.

stronger metal-support interactions expected from a reducible support, such as Fe_2O_3.[27] Accordingly, similar values as for MgO were observed with $MgAl_2O_4$ as the support (Table S8 and Figure S18). The size distribution of AuPd nanoparticles on α-Al_2O_3 (corundum) could not be established with sufficient certainty because severe contamination from Fe significantly reduced the contrast of metal nanoparticles under the electron microscope. In all cases where it was possible, the formation of alloy nanoparticles was proven by EDX line scans (Figure S19). As a side remark, the steady-state was attained in much shorter times with $MgAl_2O_4$ (Figure S9) and α-Al_2O_3 (Figure S10) as the support, probably due to the higher hardness of these materials compared to MgO, which could facilitate comminution of the metal precursors during the initial stages of the process. However, also for α-Fe_2O_3, a shorter induction period than for MgO was noted (Figure S11), although α-Fe_2O_3 (hematite) is known to be softer than MgO (periclase). Accordingly, also other factors must contribute.

Thus, if the mechanism previously described is in operation (Scheme 1), ball milling should lead to a favored state governed by surface and metal-support interaction energies. For the metal nanoparticles, this implies an interplay of opposing forces. On the one hand, the surface energy of the metal nanoparticles contributes negatively to the overall stability of the system and alone would lead to substantial coarsening to an extent depending on the nature of the metal.[29] On the other hand, favorable metal-support interactions would contribute positively to the stability of small metal nanoparticles. Overall, the results of the present study indicate that metal-support interactions are dominant in determining final metal dispersion, particularly by anchoring the nanoparticles tightly and thus limiting the kinetics of metal nanoparticles coarsening. In fact, much larger supported metal nanoparticles are expected as the thermodynamic equilibrium state, especially with MgO support.[28] Possibly, the kinetics of particle coarsening is limited depending on their corresponding interaction energy so that a quasi-steady-state is attained for different particle sizes. In this sense, the study suggests that a correct design of metal-support interactions is critical when the stability of small supported metal nanoparticles is addressed, in agreement with previous findings.[30] We are currently exploring the interplay between thermodynamic and kinetic factors in an experimental/theoretical approach for a deeper understanding of underlying phenomena.

Compared to conventional methods for the synthesis of supported catalysts, ball milling seems to adjust the thermodynamically favored state more directly since conventional methods proceed via intermediate compounds, such as nitrates, chlorides, oxides, and others related, which eventually also need to be reduced. This could mask the influence of the energetics of the metal-support system and, in turn, allow the creation of particle size distributions deviating from the thermodynamically favored one. In order to obtain deeper insight into these phenomena, quantum chemical calculations on these systems, to be carried out in the future, would be beneficial.

Conclusion

In this work, a descriptive model for the formation of supported mono- and bimetallic nanoparticles was outlined as a result of systematic investigations extended to many different metals and oxide supports. It was observed that metal comminution proceeds with a rate depending on the nature of the metal and the support oxide, respectively. Particularly, the difference in the intrinsic mechanical properties of metals and metal oxides accounts for the trends observed during the comminution stage. The relative affinity (oxophilicity) of the metals for the given oxide support explains the final metal dispersions, which were obtained after prolonged ball milling. Alloying of metal nanoparticles was only noted after a high level of dispersion had already been attained for the metal species. From this point onwards, alloying proceeds with the gradual dissolution of one component into the other until a steady-state is attained. No specific sign of preferential mixing was noted. Finally, a mechanism for the coalescence of metal nanoparticles was proposed.

The study also resulted in the synthesis of an expanded scope of materials, which proves the rather general applicability of dry ball milling for the synthesis of supported mono- and bimetallic nanoparticles. Furthermore, the method is quite tolerant concerning the choice of metal(s), alone and in combination, and oxide supports. Notably, the preparation of hard-to-synthesize PdPt and PtAu disordered alloys (as supported nanoparticles) was achieved under mechanochemical conditions. Finally, different mixing patterns were noted for the alloy species depending on the milling time and milling frequency, suggesting that the tuning of such parameters could provide an additional level of control for the synthesis.

Acknowledgements

Max-Planck-Institut für Kohlenforschung is acknowledged for financial support. Marc Meyer is acknowledged for his assistance with the preparation of the samples. Further, we are grateful to Silvia Palm and Alexander Kostis for the SEM-EDX bulk elemental analysis of the samples and to Adrian Schlüter for the assistance with the electron microscopy analysis (TEM). Finally, the technical support from the fine mechanic workshop led by Wolfgang Kersten was crucial to the success of the study. Open Access funding enabled and organized by Projekt DEAL.

Conflict of Interest

The authors declare no conflict of interest.

Data Availability Statement

The data that support the findings of this study are available from the corresponding author upon reasonable request.

Keywords: Ball Milling · Bimetallic Nanoalloys · Metal Nanoparticles · Solvent-Free Synthesis · Supported Catalysts

[1] L. Liu, A. Corma, *Chem. Rev.* **2018**, *118*, 4981–5079.
[2] J. Shi, *Chem. Rev.* **2013**, *113*, 2139–2181.
[3] O. G. Ellert, M. V. Tsodikov, S. A. Nikolaev, V. M. Novotortsev, *Russ. Chem. Rev.* **2014**, *83*, 718–732.
[4] X. Huang, O. Akdim, M. Douthwaite, K. Wang, L. Zhao, R. J. Lewis, S. Pattisson, I. T. Daniel, P. J. Miedziak, G. Shaw, D. J. Morgan, S. M. Althahban, T. E. Davies, Q. He, F. Wang, J. Fu, D. Bethell, S. McIntosh, C. J. Kiely, G. J. Hutchings, *Nature* **2022**, *603*, 271–275.
[5] a) H.-L. Jiang, Q. Xu, *J. Mater. Chem.* **2011**, *21*, 13705–13725; b) A. K. Singh, Q. Xu, *ChemCatChem* **2013**, *5*, 652–676.
[6] a) M. Sankar, N. Dimitratos, P. J. Miedziak, P. P. Wells, C. J. Kiely, G. J. Hutchings, *Chem. Soc. Rev.* **2012**, *41*, 8099–8139; b) Z. Wei, J. Sun, Y. Li, A. K. Datye, Y. Wang, *Chem. Soc. Rev.* **2012**, *41*, 7994–8008.
[7] P. Munnik, P. E. de Jongh, K. P. de Jong, *Chem. Rev.* **2015**, *115*, 6687–6718.
[8] a) K. Ralphs, C. Hardacre, S. L. James, *Chem. Soc. Rev.* **2013**, *42*, 7701–7718; b) C. Xu, S. De, A. M. Balu, M. Ojeda, R. Luque, *Chem. Commun.* **2015**, *51*, 6698–6713; c) A. P. Amrute, J. De Bellis, M. Felderhoff, F. Schüth, *Chem. Eur. J.* **2021**, *27*, 6819–6847; d) T. Tsuzuki, *Commun. Chem.* **2021**, *4*, 143; e) J. Zhao, J. Bao, S. Yang, Q. Niu, R. Xie, Q. Zhang, M. Chen, P. Zhang, S. Dai, *ACS Catal.* **2021**, *11*, 12247–12257; f) Y. Shu, M. Wang, X. Duan, D. Liu, S. Yang, P. Zhang, *AIChE J.* **2022**, *68*, e17664.
[9] H. Schreyer, R. Eckert, S. Immohr, J. De Bellis, M. Felderhoff, F. Schüth, *Angew. Chem. Int. Ed.* **2019**, *58*, 11262–11265; *Angew. Chem.* **2019**, *131*, 11384–11387.
[10] J. De Bellis, M. Felderhoff, F. Schüth, *Chem. Mater.* **2021**, *33*, 2037–2045.
[11] a) A. Mussio, M. Danielis, N. J. Divins, J. Llorca, S. Colussi, A. Trovarelli, *ACS Appl. Mater. Interfaces* **2021**, *13*, 31614–31623; b) R. T. P. da Silva, S. I. Córdoba De Torresi, P. F. M. de Oliveira, *Front. Chem.* **2022**, *10*, 836597.
[12] a) U. Kamolphop, S. F. R. Taylor, J. P. Breen, R. Burch, J. J. Delgado, S. Chansai, C. Hardacre, S. Hengrasmee, S. L. James, *ACS Catal.* **2011**, *1*, 1257–1262; b) M. Danielis, S. Colussi, C. de Leitenburg, L. Soler, J. Llorca, A. Trovarelli, *Angew. Chem. Int. Ed.* **2018**, *57*, 10212–10216; *Angew. Chem.* **2018**, *130*, 10369–10373.
[13] O. V. Lapshin, E. V. Boldyreva, V. V. Boldyrev, *Russ. J. Inorg. Chem.* **2021**, *66*, 433–453.
[14] P. Scardi, M. Leoni, *Acta Crystallogr. Sect. A* **2002**, *58*, 190–200.
[15] S. Kibey, J. B. Liu, D. D. Johnson, H. Sehitoglu, *Acta Mater.* **2007**, *55*, 6843–6851.
[16] A. D. Pandey, R. Güttel, M. Leoni, F. Schüth, C. Weidenthaler, *J. Phys. Chem. C* **2010**, *114*, 19386–19394.
[17] a) H. Okamoto, T. B. Massalski, *Bull. Alloy Phase Diagrams* **1985**, *6*, 229–235; b) I. Karakaya, W. T. Thompson, *Bull. Alloy Phase Diagrams* **1988**, *9*, 237–243.
[18] S. M. Foiles, M. I. Baskes, M. S. Daw, *Phys. Rev. B* **1986**, *33*, 7983–7991.
[19] M. M. Mariscal, S. A. Dassie, E. P. M. Leiva, *J. Chem. Phys.* **2005**, *123*, 184505.
[20] L. Aymard, A. Delahaye-Vidal, F. Portemer, F. Disma, *J. Alloys Compd.* **1996**, *238*, 116–127.
[21] P. Baláž, *Mechanochemistry in Nanoscience and Minerals Engineering*, Springer, Berlin, Heidelberg, **2008**.
[22] a) K. Užarević, I. Halasz, T. Friščić, *J. Phys. Chem. Lett.* **2015**, *6*, 4129–4140; b) P. F. M. de Oliveira, A. A. L. Michalchuk, A. G. Buzanich, R. Bienert, R. M. Torresi, P. H. C. Camargo, F. Emmerling, *Chem. Commun.* **2020**, *56*, 10329–10332; c) J. G. Schiffmann, F. Emmerling, I. C. B. Martins, L. Van Wüllen, *Solid State Nucl. Magn. Reson.* **2020**, *109*, 101687; d) G. I. Lampronti, A. A. L. Michalchuk, P. P. Mazzeo, A. M. Belenguer, J. K. M. Sanders, A. Bacchi, F. Emmerling, *Nat. Commun.* **2021**, *12*, 6134; e) H. Petersen, S. Reichle, S. Leiting, P. Losch, W. Kersten, T. Rathmann, J. Tseng, M. Etter, W. Schmidt, C. Weidenthaler, *Chem. Eur. J.* **2021**, *27*, 12558–12565; f) T. Rathmann, H. Petersen, S. Reichle, W. Schmidt, A. P. Amrute, M. Etter, C. Weidenthaler, *Rev. Sci. Instrum.* **2021**, *92*, 114102.
[23] R. F. Zhang, X. F. Kong, H. T. Wang, S. H. Zhang, D. Legut, S. H. Sheng, S. Srinivasan, K. Rajan, T. C. Germann, *Sci. Rep.* **2017**, *7*, 9577.
[24] a) H. Okamoto, T. B. Massalski, *Bull. Alloy Phase Diagrams* **1985**, *6*, 46–56; b) S. R. Bharadwaj, A. S. Kerkar, S. N. Tripathi, S. R. Dharwadkar, *J. Less-Common Met.* **1991**, *169*, 167–172.
[25] R. Ferrando, J. Jellinek, R. L. Johnston, *Chem. Rev.* **2008**, *108*, 845–910.
[26] C. Suryanarayana, *Prog. Mater. Sci.* **2001**, *46*, 1–184.
[27] S. L. Hemmingson, C. T. Campbell, *ACS Nano* **2017**, *11*, 1196–1203.
[28] Z. Mao, C. T. Campbell, *ACS Catal.* **2021**, *11*, 8284–8291.
[29] L. Vitos, A. V. Ruban, H. L. Skriver, J. Kollár, *Surf. Sci.* **1998**, *411*, 186–202.
[30] J. A. Farmer, C. T. Campbell, *Science* **2010**, *329*, 933–936.

Manuscript received: May 31, 2022
Accepted manuscript online: August 16, 2022
Version of record online: August 29, 2022